








Ocean bottom seismic model in the Knipovich Ridge area

Wojciech CZUBA^{1*} , Yoshio MURAI² , Tomasz JANIK¹ ,
Andrzej GÓRSZCZYK¹  and Krzysztof MICHALSKI¹ 

¹ *Institute of Geophysics, Polish Academy of Sciences, Ks. Janusza 64, 01-452 Warszawa, Poland*

² *Hokkaido University, Kita 8, Nishi 5, Kita-ku, Sapporo, Hokkaido, 060-0808 Japan*

corresponding author: wojt@igf.edu.pl

Received 13 June 2025 Accepted 29 September 2025

Abstract: The structure of the oceanic crust generated by the ultraslow-spreading mid-ocean Knipovich Ridge still remains relatively uninvestigated compared to the other North Atlantic spreading ridges further south. The complexity of the Knipovich Ridge, with its oblique ultraslow-spreading and segmentation, makes this end-member of Spreading Ridge Systems an important and challenging ridge to investigate. The Ocean Bottom Seismometer (OBS) data along a refraction/reflection profile (*ca.* 280 km) crossing the Knipovich Ridge off the western Barents Sea was acquired during cruise of RV G.O. Sars on July 24 to August 6, 2019. The seismic energy was emitted by air-guns with total volume of 80 l. To receive and record the seismic waves at the seafloor, ocean bottom seismometers were deployed. Seismic energy from airgun shots were recorded up to 50 km from the OBSs. The profile provides information on the seismic structure of the oceanic crust in the Knipovich Ridge area. Seismic record sections were analyzed with 2D trial-and-error forward seismic modeling. The crust thickness is variable and the Moho boundary depth changes between 7 and 12 km with P-wave velocity below the interface 7.9–8.0 km/s. The Moho discontinuity attains its minimum depth not directly beneath the Knipovich Ridge, but roughly 30 km to the southeast.

Keywords: Arctic, North Atlantic, seismic model, oceanic crust.

Introduction

The oceanic crust, which covers *ca.* 60% of the Earth's surface, is created along the mid-ocean ridge (MOR) systems. Oceanic crust created at the MORs where spreading rate exceeds 20 mm/yr is comparatively uniform and *ca.* 6–7 km thick (White *et al.* 2001; Van Avendonk *et al.* 2017). On the other hand, ultraslow-spreading ridges (<20 mm/y) form a unique category of MORs in terms of crustal thickness, structure and geochemical composition (Dick *et al.* 2003; Grevemeyer *et al.* 2018). Most current models assume that passive mantle upwelling is the dominant mechanism of melt generation in these unique rift environments (Dick *et al.* 2003).

Ultraslow-spreading MORs can be found in both hemispheres. However, the two most extensive ultraslow-spreading systems are the Arctic Ridge system in the Northern Atlantic Ocean to which the Knipovich Ridge belongs, and the Southwest Indian Ridge in the Indian Ocean. The Knipovich Ridge, with a spreading rate not exceeding 13 mm/yr, is a classic example of an ultra-

slow-spreading MOR (Dumais *et al.* 2021; Meier *et al.* 2022).

The few existing seismic studies prove that the average crustal thickness at ultraslow-spreading ridges is rather low, *i.e.*, 2–5 km (Ritzmann *et al.* 2002; Jokat and Schmidt-Aursch 2007; Hermann and Jokat 2013). The Knipovich Ridge is relatively easily accessible for seismic surveys, but due to the obliquity in the spreading direction and segmentation it is characterized by a high complexity, which makes it an important and challenging ridge to investigate (Curewitz *et al.* 2010).

High-resolution seismic imaging, particularly through large-scale installations of ocean-bottom seismometers (OBS), provides essential constraints on the structure of the crust and upper mantle. These methods are critical for delineating the geometry of the crust–mantle boundary, *i.e.*, the Moho, and identifying regions of partial melt and lithospheric thinning. In this study, we present the new KNIPSEIS OBS profile (Fig. 1) which provides data on the seismic structure of the crust in the Knipovich Ridge and the North Atlantic Ocean towards south-east. The



oceanic crust formed in the ultraslow-spreading Knipovich Ridge is still a relatively unexplored area compared to the other North Atlantic spreading ridges further south. This investigation presents an analysis of wide-angle reflection and refraction (WARR) seismic profile performed in the frame of the KNIPSEIS Project in 2019 to study active spreading processes and lithospheric structure of the ridge.

Study area

The Knipovich Ridge (73°50'N to 78°30'N; Fig. 1) is a section of the Mid-Atlantic Ridge (MAR) system, and its formation is associated with the northward propagation of the MAR during the Cenozoic (Gernigon *et al.* 2020; Gaina *et al.* 2025). The North Atlantic Ocean started its opening process in the Early Eocene 54.6 Ma ago with successive spreading of Reykjanes, Aegir and Mohs ridges (Talwani and Eldholm 1977). The Knipovich Ridge (Fig. 1) started its development *ca.* 23 Ma ago as the propagation of the northern MAR towards the Spitsbergen Shear Zone (Kandilarov *et al.* 2010). The Knipovich Ridge stretches from 73°30'N in the south, where it connects to the Mohs Ridge, up to 78°30'N where it terminates in the Molloy Fracture Zone (Kandilarov *et al.* 2010). The spreading rate of the northern Knipovich Ridge is 14 mm/year (DeMets *et al.* 1990). The Knipovich Ridge is characterized by a heterogeneous assemblage of magmatic and amagmatic segments, which co-exist in a patchwork-like pattern along the ridge axis (Helleberg and Pedersen 2005; Meier *et al.* 2022).

Seismic experiments with controlled sources in the Knipovich Ridge are relatively modest compared with better examined ultraslow-spreading Southwest Indian Ridge, however, it is worth to mention several seismic projects that have been carried out in this region so far. One of the first WARR profiles crossing the Knipovich Ridge is the K1 profile conducted in 1985 (Czuba *et al.* 1999). In the subsequent years, further seismic profiles were acquired, such as the line AWI-97260, extended towards west by profile 9_98 (Ritzmann *et al.* 2002) and profile 8_98 conducted in 1998 (Ljones *et al.* 2004), and extended in 2005 by profile Horsted'05 (Czuba *et al.* 2008; Krysiński *et al.* 2013). Those profiles are valuable sources of information about the thickness of the crust, segmentation and first assumptions of mantle serpentinization of the ultraslow-spreading Knipovich Ridge. In 2009, the AWI-20090200 profile was realized (Hermann and Jokat 2013), which SE end crosses the Knipovich Ridge in the same place as the KNIPSEIS profile NW end.

Methods

The OBS data along a KNIPSEIS profile (*ca.* 280 km), crossing the Knipovich Ridge off the western Barents Sea, was collected by the Norwegian vessel RV G.O. Sars on July 24 to August 6, 2019. The airgun array (80 l total volume) emitted seismic energy every 200 m. In order to receive and record the seismic signal at the seafloor, ocean bottom seismometers were installed at 12 positions with

ca. 15-km spacing in two deployments (Fig. 1). Seismic energy from airgun shots was recorded up to a distance of 50 km, and in some cases, even further. Several OBSs revealed clear arrivals beyond 100 km offset.

During the first deployment, 4 Guralp broadband OBSs maintained by the Polish team and 5 short-period Norwegian OBSs maintained by the Japanese-Polish team were used. RV G.O. Sars performed the shooting along the profile. Then all the Guralp OBSs were retrieved and 3 of them were deployed at the other end of the profile, after the short-period OBSs, which stayed on the seafloor (Fig. 1). The airgun shooting was performed again along the profile.

The location of all shots and seismic receivers was determined and synchronised using a GPS system. All stations recorded continuously during the experiment. All the data were successfully downloaded. In the pre-processing procedure, all records were resampled to 100 Hz and cut into single 60 s long time traces, with "zero" time at original shot time. A band-pass filter of 5–18 Hz was usually used during processing and interpretation. Preparation of the data for modelling required information on the exact location of each OBS. During the acquisition, it was impossible to triangulate their positions and therefore relocation was required. The relocation procedure was based on an assumption that branches of the water wave, observed on receiver gathers with correct OBS coordinates, should be symmetrical. During the relocating procedure, the distances between OBS and traces were recalculated until the water wave branches became symmetrical.

In general, the signal to noise ratio at short-offsets channels is high. However, with increasing source-receiver distance we observe rapid decrease of the signal energy, which becomes dominated by the random noise. This is especially visible for the first arrivals, which for some OBS are significantly attenuated by the water-wave. We first applied predicting deconvolution (Peacock and Treitel 1969) to reduce the bubble effect. To increase signal coherency, we essentially tested three filtering methods based on: (i) discrete curvelet transform (Górszczyk *et al.* 2014); (ii) multichannel convolution filter (Trojanowski *et al.* 2016); and (iii) f-x deconvolution (Canales 1984). The first two techniques, although they strongly attenuated the noise, introduced notable artefacts in the areas of weak signal. Therefore, we decided to use the f-x deconvolution, which led to the most satisfying results in terms of noise reduction and signal preservation.

A 2D crustal velocity model was derived using a ray-tracing technique from all P-wave phases available. The identification and correlation of seismic phases were conducted manually on a computer display using the ZPLOT software, which facilitates scaling, filtering and velocity reduction (Zelt 1994). Travel times, ray paths and synthetic seismograms calculation was conducted utilising the SEIS83 package (Červený and Pšenčík 1983), augmented by the interactive graphical interface MODEL (Komminaho 1997). The initial input for two-dimensional modelling was the ocean water layer, the thickness of which was measured

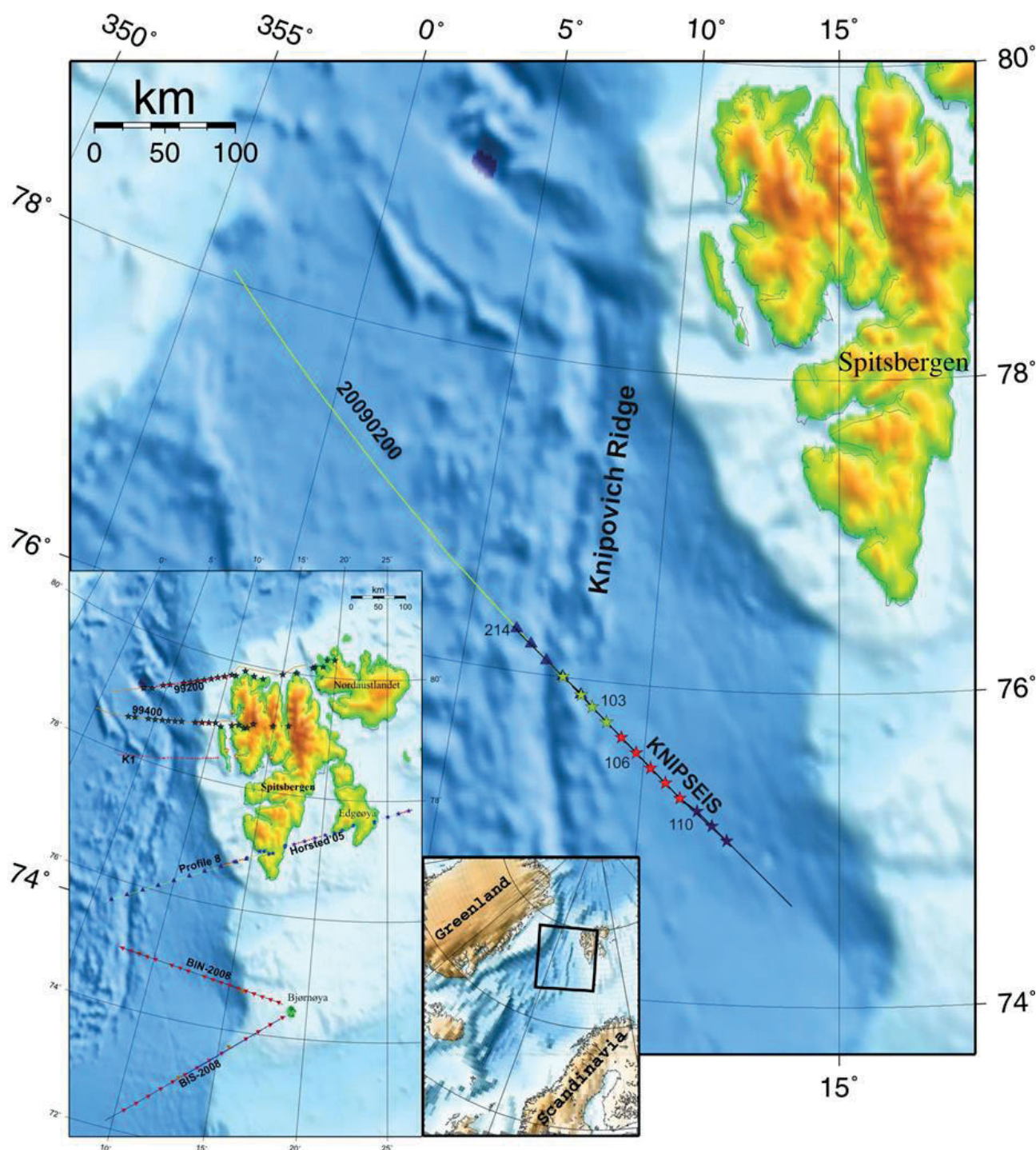


Fig. 1. Location map of the seismic profile KNIPSEIS on top of topography/bathymetry map (Jakobsson *et al.* 2000). Thin line marks airgun shots, triangles (20090200, Hermann and Jokat 2013) and stars (this profile) are seismic OBS stations. Red stars – Japanese OBSs, green stars – first deployment of the Polish OBSs, dark blue stars – second deployment of the Polish OBSs. Numbers are OBS names. The black rectangle in the small inset marks the area of the main map. Left bottom inset – a map with old profiles. The public domain GMT software (Wessel and Smith 1998; Wessel *et al.* 2013) was used to produce the map with the profile.

during the cruise. The initial P-wave velocity for the water layer was assumed to be 1500 m/s, which underwent minor adjustments during the modelling process. The final velocity value was found to be within the range of 1460–1480 m/s, which is representative of typical sound speeds in the Norwegian-Greenland Sea (Mjelde *et al.* 2002).

The two-dimensional velocity model for sediments, crystalline crust and crust-mantle transition was subject to successive alterations through a process of trial and error. The travel times for the consecutive layers were recalculated multiple times until obtained observed (picked) and model-derived travel times agreed. Concurrently with the

kinematic modelling, synthetic seismograms were calculated to regulate velocity gradients within the layers and velocity contrasts across seismic boundaries.

The quality of the data is generally satisfactory thus enabling detailed wave field analysis and crustal structure modelling to be conducted. All P-wave record sections are presented in Figs. 2–5. Figs. 6–8 show examples of seismic modelling presenting together travel times, rays and synthetic sections calculated for the 2D crustal velocity model (Fig. 9). Seismic energy recorded from the oceanic crust and uppermost mantle are much weaker than water waves. The phase identification process is complicated by the presence of relatively strong reverberations and a considerable amount of noise in certain locations. To address this issue, manual removal of the noisiest traces from the record sections was undertaken. In the subsequent phases of the data interpretation, including the correlation of seismic phases, a range of plot methods and visualizations were employed. The application of band-pass filters, zooms and changes in amplification to different parts of the record sections was intended to extract and display the clearest signal arrivals, thus making arrival time picking more accurate.

Results

Examples of normalized record section plots from airgun shots are shown in Figs. 2–5. Examples of the wave field together with calculated travel times, ray diagram and synthetic section are presented in Figs. 6–8. We can observe significant distinctions between the NW and SE segments of the profile. A complicated shape of arrivals and quite early crustal and mantle P-wave branches can be visible at NW receivers (OBS 101–103, Fig. 2). It seems to be a mantle velocity (*ca.* 8 km/s) just at OBS 103 at about 3 s reduced time. In this area, probably, the shallowest Moho interface could be found. These OBSs recorded lowest quality arrivals, probably because of the most complicated crustal structure. Figure 3 (OBS 104–106) shows a transition zone between the ridge and the quite smooth oceanic crust to SE. The best example is OBS 106 where to NW (left side) a complicated P-wave arrivals shape with quite early high apparent velocities are visible. In contrary, at right side (toward SE) the apparent P-wave velocities are lower and respective arrivals are later, quite simply and rather flat. Records from OBSs 107–112 (Figs. 4 and 5) are characterized by long branches with low apparent P-wave velocities and then quite flat branches at *ca.* 5 s reduced travel time, with P-wave apparent velocity being *ca.* 8 km/s.

Modelling examples are shown on Figs. 6–8. There are measured seismic record sections with labelled calculated travel times. A ray diagram through seismic model is shown as well as a synthetic seismic section indicating relative amplitudes fit. The synthetic seismograms show good qualitative agreement of the relative amplitudes of observed refracted and reflected waves with the synthetic record sections. There are some sedimentary branches

(P_{sed}) with low apparent P-wave velocity at every OBS. The longest branches from sediments are modelled in the central and SE part of the profile (Figs. 7 and 8). The branches of crustal phases (P_g) are rather short, which indicates quite thin crust. The P-wave apparent velocity is higher in the SE part of the profile (Fig. 8). It is worth to note that high crustal velocity of *ca.* 7 km/s is visible NW from OBS110 (Fig. 8). It is very hard to model Moho reflections (P_{MP}). They are relatively weak and therefore hard to pick. An example is shown on Figs. 7 and 8 (OBS 106 and 110) in the SE part of the profile, far from the ridge. It can be interpreted as weak reflectivity (rather transition) at the Moho interface near the ridge axis. The upper mantle refractions (P_n and P_1) are modelled rather close to an OBS 103 (*ca.* 20 km) with lower apparent P-wave velocity (*ca.* 7 km/s) in the NW (ridge) part of the profile (Fig. 6) and higher to the SE, reaching at least 8 km/s (Figs. 7 and 8). The reduced arrival time is earlier in the ridge axis area (3–4 s on Figs. 6 and 7), while it is later further towards SE (*ca.* 5 s on Figs. 7 and 8). This suggests lower P-wave velocity beneath the Moho interface and thinner crust in the ridge area.

Because of offshore location of the measurement line, all shots and OBS receivers were in-line (Fig. 1). Using modern GPS techniques, the shot and record times as well as locations of shots were measured very precisely, on the order of 1 ms and tens of meters, respectively. Such errors are insignificant in a crustal-scale experiment. OBSs were relocated using their precise recordings. Uncertainties of velocity and depth in the model obtained using the ray tracing technique result first of all from the uncertainties of subjectively picked travel times. However, it is important to note that the accuracy of these measurements increases with increasing quality and amount of the data available. This includes the number of shots and receivers, the effectiveness of sources, the signal-to-noise ratio, the reciprocity of travel time branches, and the ray coverage in the model. In the context of offshore experiments, the presence of water multiples, multiples of P- and S-waves, and converted P-to-S waves introduces additional complications. When interpreted incorrectly, they have the potential to result in serious mistakes, the magnitude of which is challenging to predict.

In case of optimal quality of data and interpretation, the implementation of ray tracing method yielded theoretical travel times that exhibited satisfactory correspondence with the observed (experimental) travel times for both refracted and reflected waves. It was estimated that the inaccuracy of the picking time is *ca.* 0.1 s. Velocities are modelled with accuracy of the order of 0.1 km/s for first arrivals and the Moho depth accuracy is *ca.* 1–2 km. Extensive tests were performed for this modelling method in Janik *et al.* (2002), Mjelde *et al.* (2002), Grad *et al.* (2003, 2006, 2008) and Środa *et al.* (2006).

The 2D raytracing seismic modelling resulted in a seismic P-wave velocity model along the line (Fig. 9). This is a prolongation of the previously realized project (Hermann and Jokat 2013), so the distance axis runs from the begin-

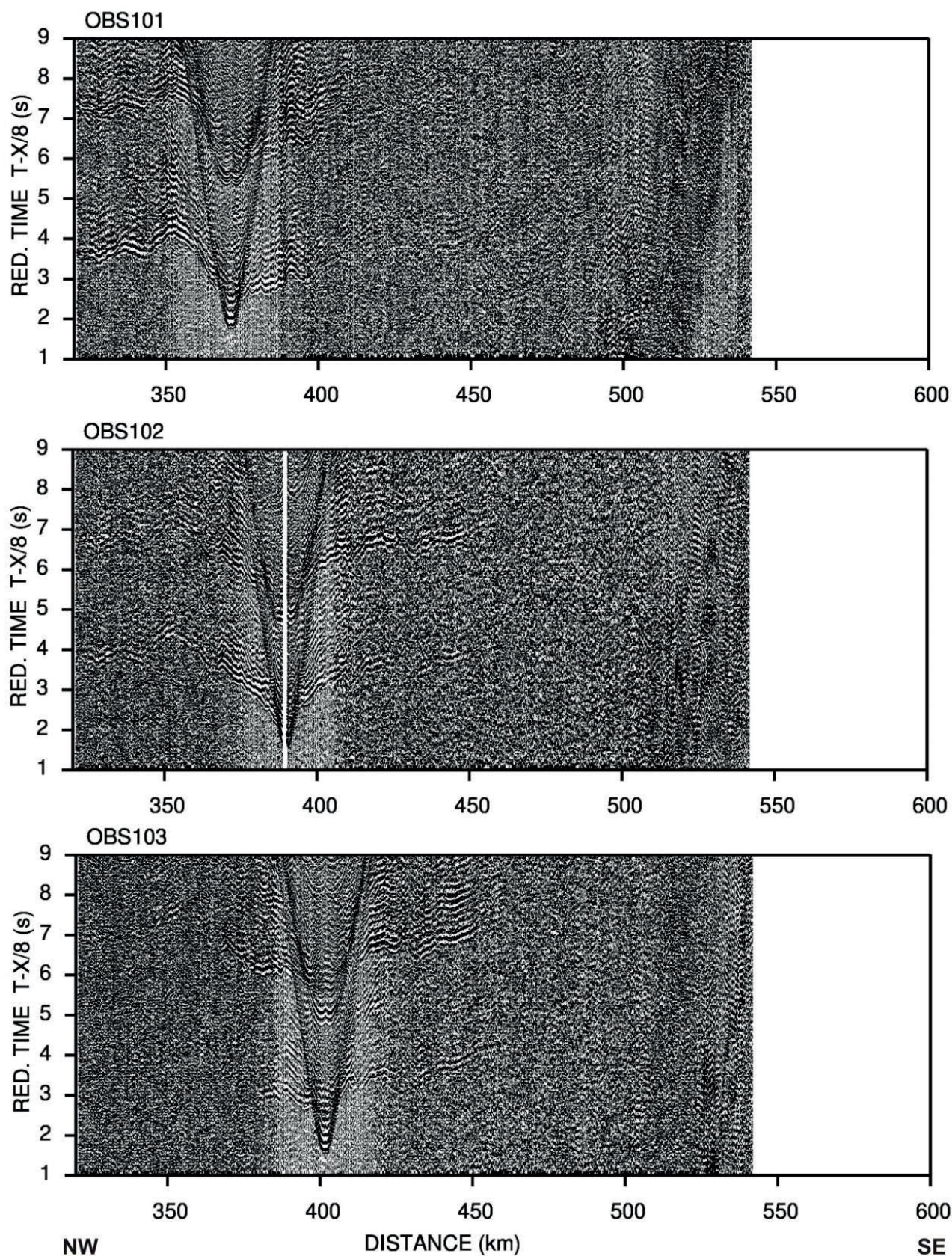


Fig. 2. Amplitude-normalized, vertical-component seismic record sections recorded by OBSs 101–103 during the KNIPSEIS project. Band-pass filtration is 5–18 Hz and velocity reduction 8 km/s.

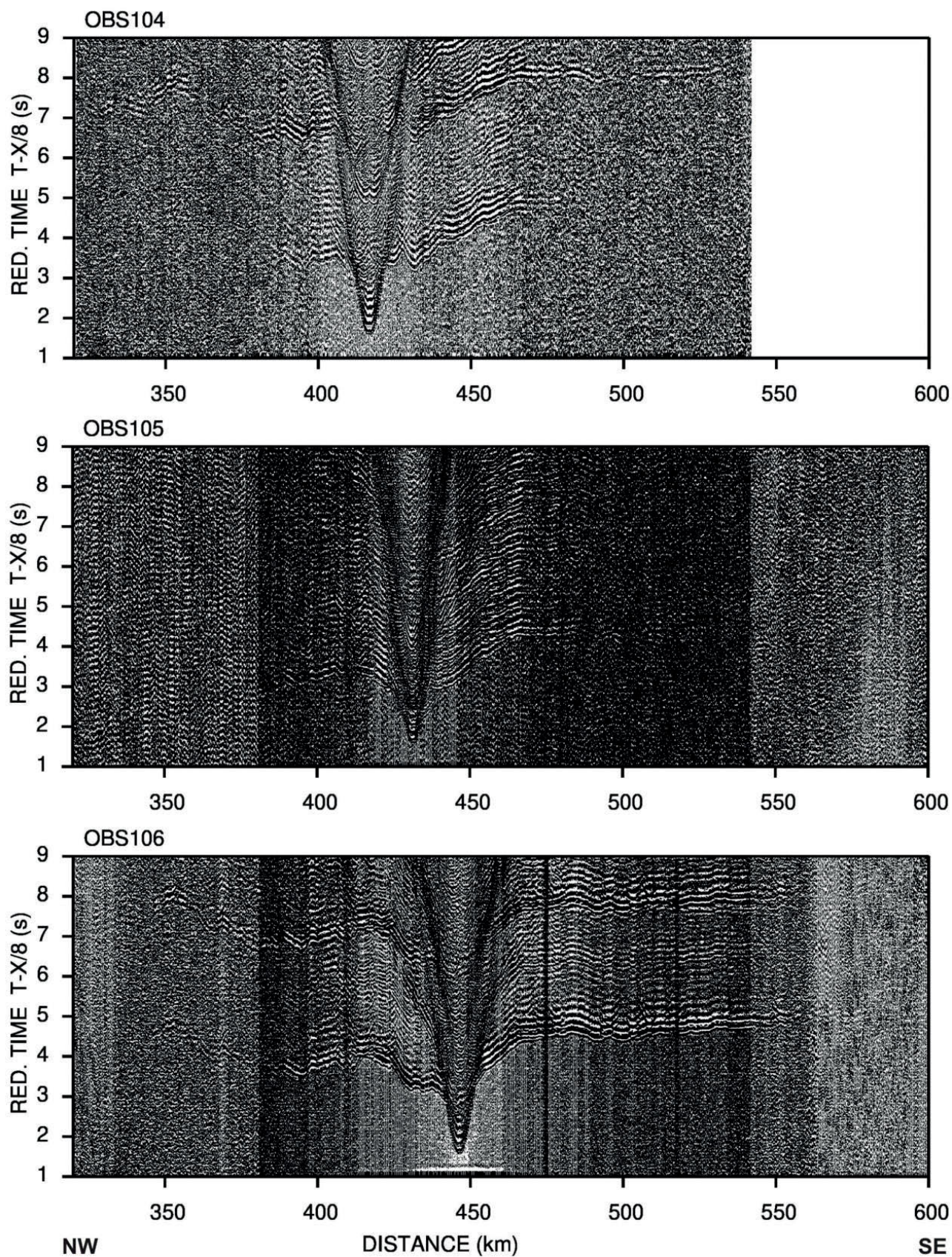


Fig. 3. Amplitude-normalized, vertical-component seismic record sections recorded by OBSs 104–106 during the KNIPSEIS project. Band-pass filtration is 5–18 Hz and velocity reduction 8 km/s.

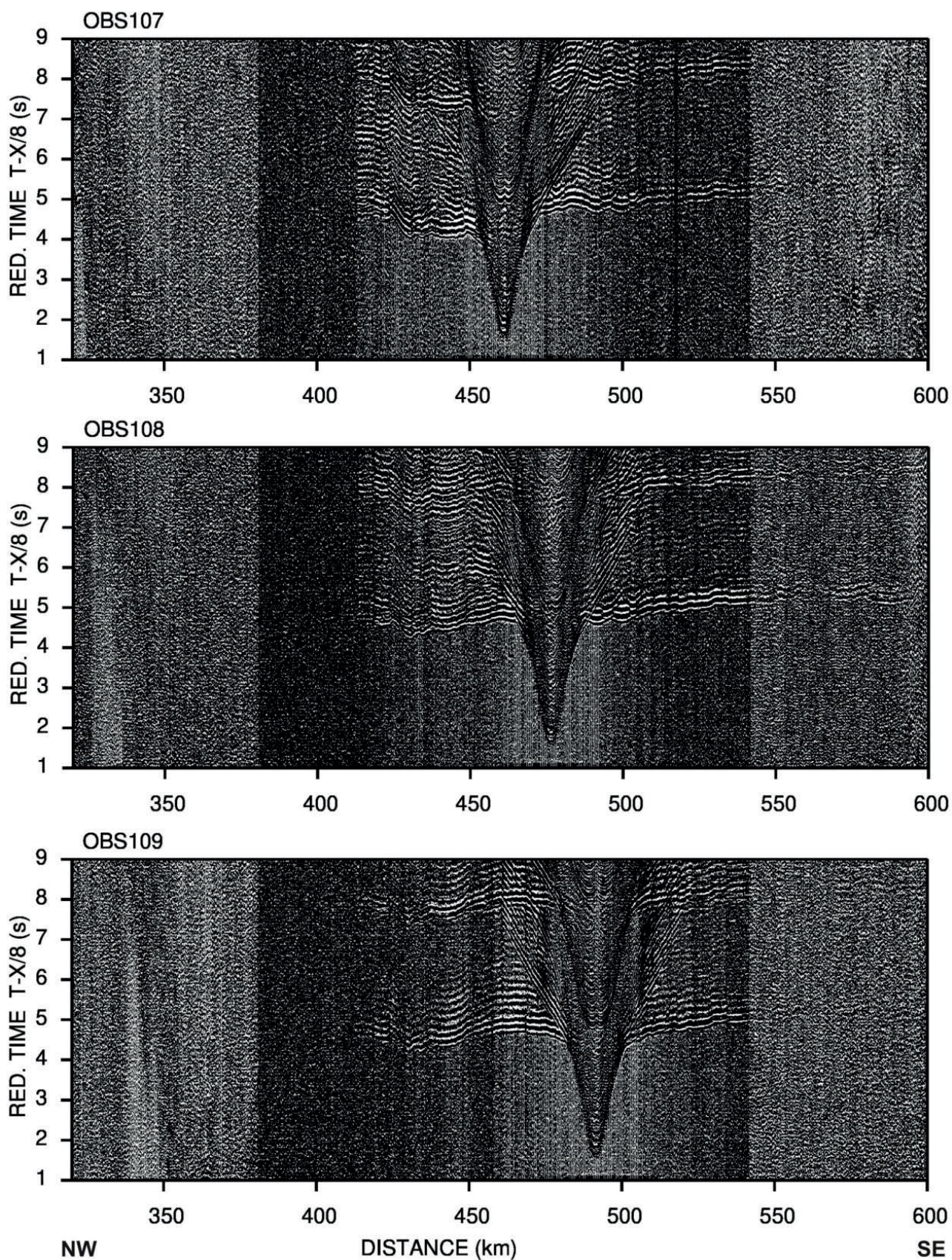


Fig. 4. Amplitude-normalized, vertical-component seismic record sections recorded by OBSs 107–109 during the KNIPSEIS project. Band-pass filtration is 5–18 Hz and velocity reduction 8 km/s.

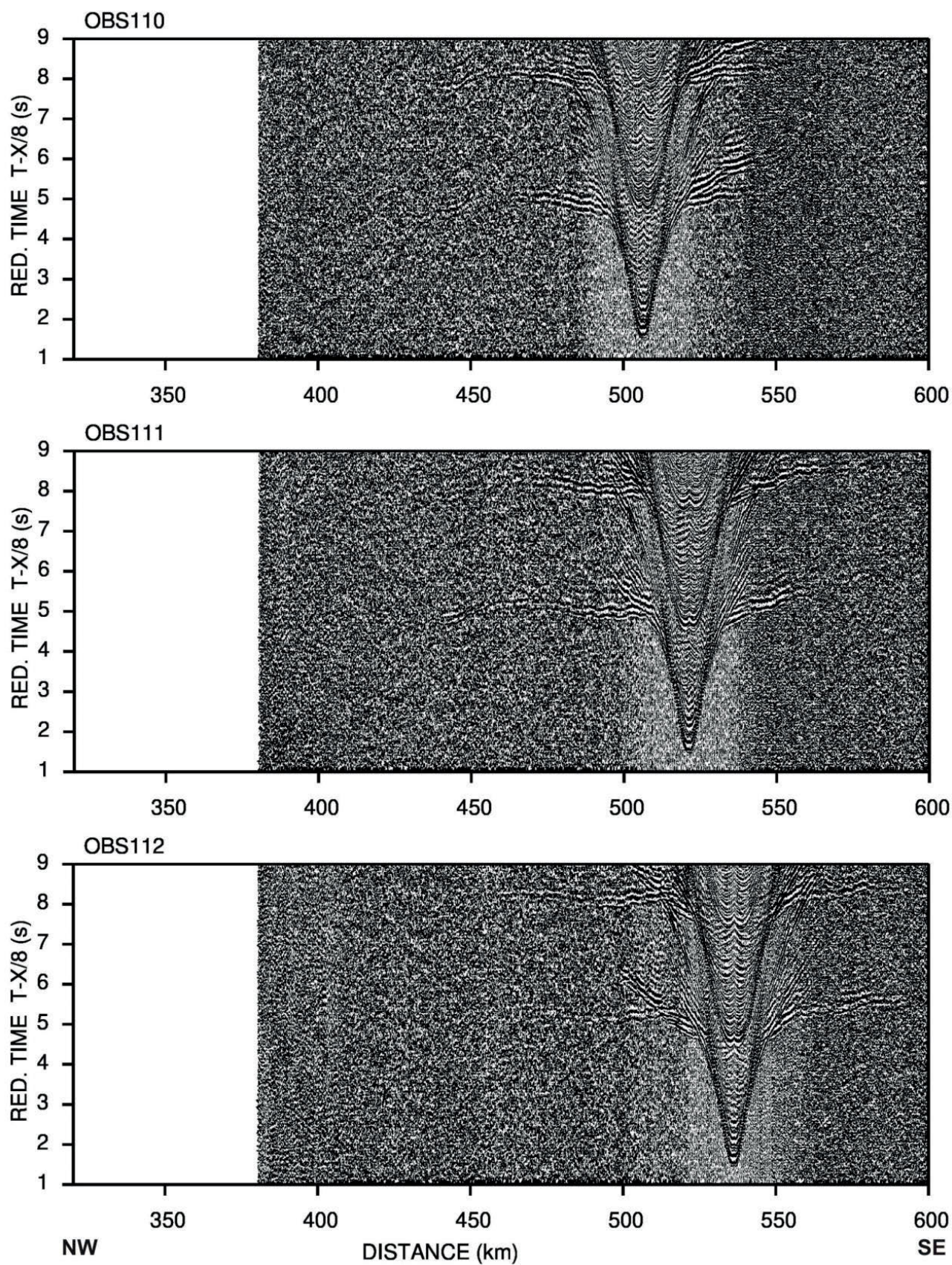


Fig. 5. Amplitude-normalized, vertical-component seismic record sections recorded by OBSs 110–112 during the KNIPSEIS project. Band-pass filtration is 5–18 Hz and velocity reduction 8 km/s.

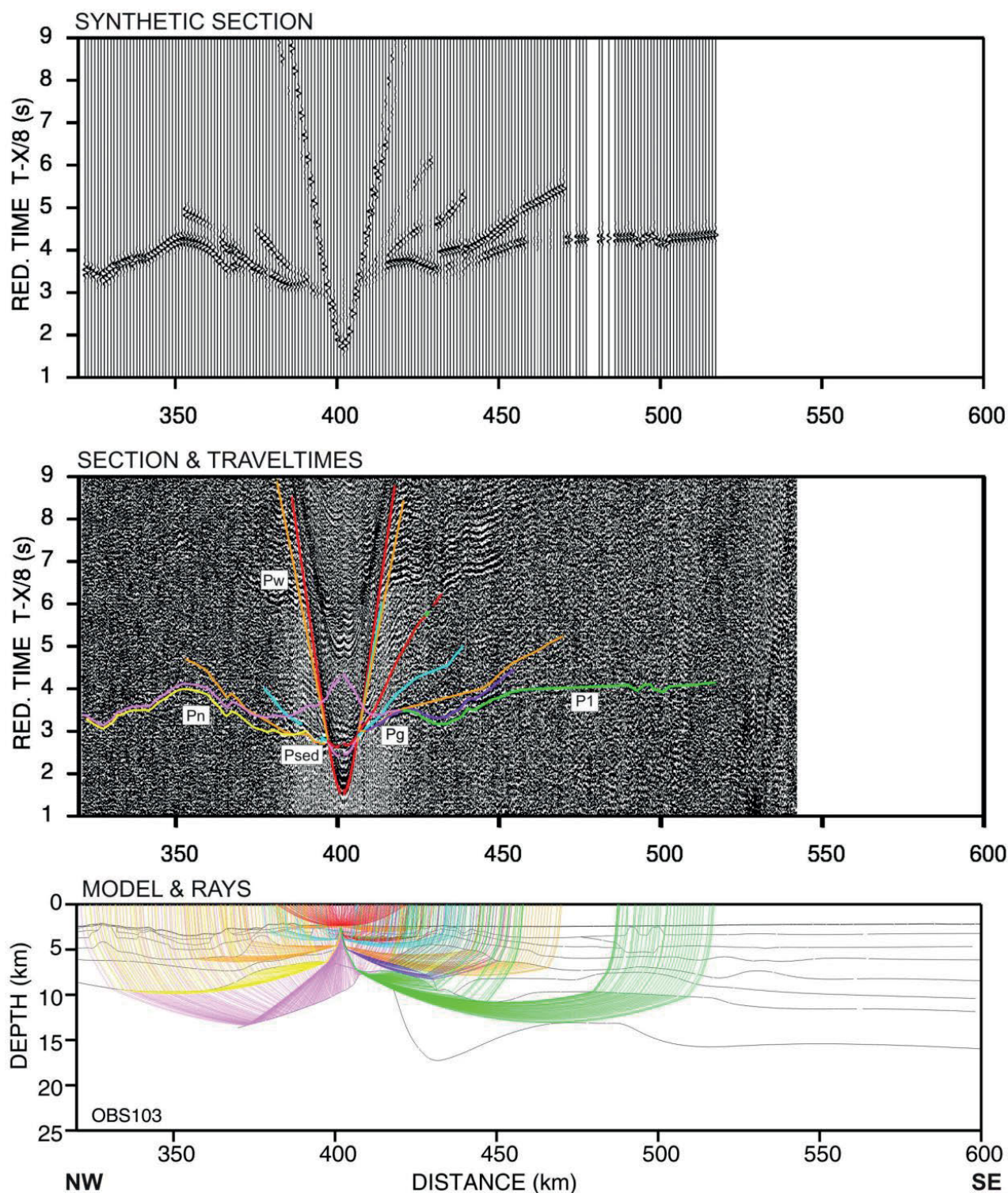


Fig. 6. Example of the 2-D seismic modelling along the KNIPSEIS profile for amplitude-normalized record section of OBS 103: model with rays (bottom), observed record sections (vertical-component) with calculated travel times (middle) and synthetic seismograms (top). Colours of calculated travel times correspond to ray colours in the ray diagram. Band-pass filtration is 5–18 Hz and velocity reduction is 8 km/s. Pw – water waves; Psed – first arrivals of P-waves travelling through sediments; Pg – first arrivals of crustal P-waves; Pn – refracted P-waves beneath the Moho; P1 – lower lithospheric reflections. For the final seismic model see Fig. 9.

ning of that profile (AWI-200990200). The last five OBSs (214–218) from that profile were adopted for this modelling, up to the limit of KNIPSEIS shooting line. The presented model depicts the oceanic crustal structure toward

the SE as comprising several parallel layers, with P-wave velocities increasing from 1.95 km/s at the seafloor to 7.20 km/s at the Moho boundary, located at a depth of *ca.* 12 km. The thickness of the upper crustal layers is up to

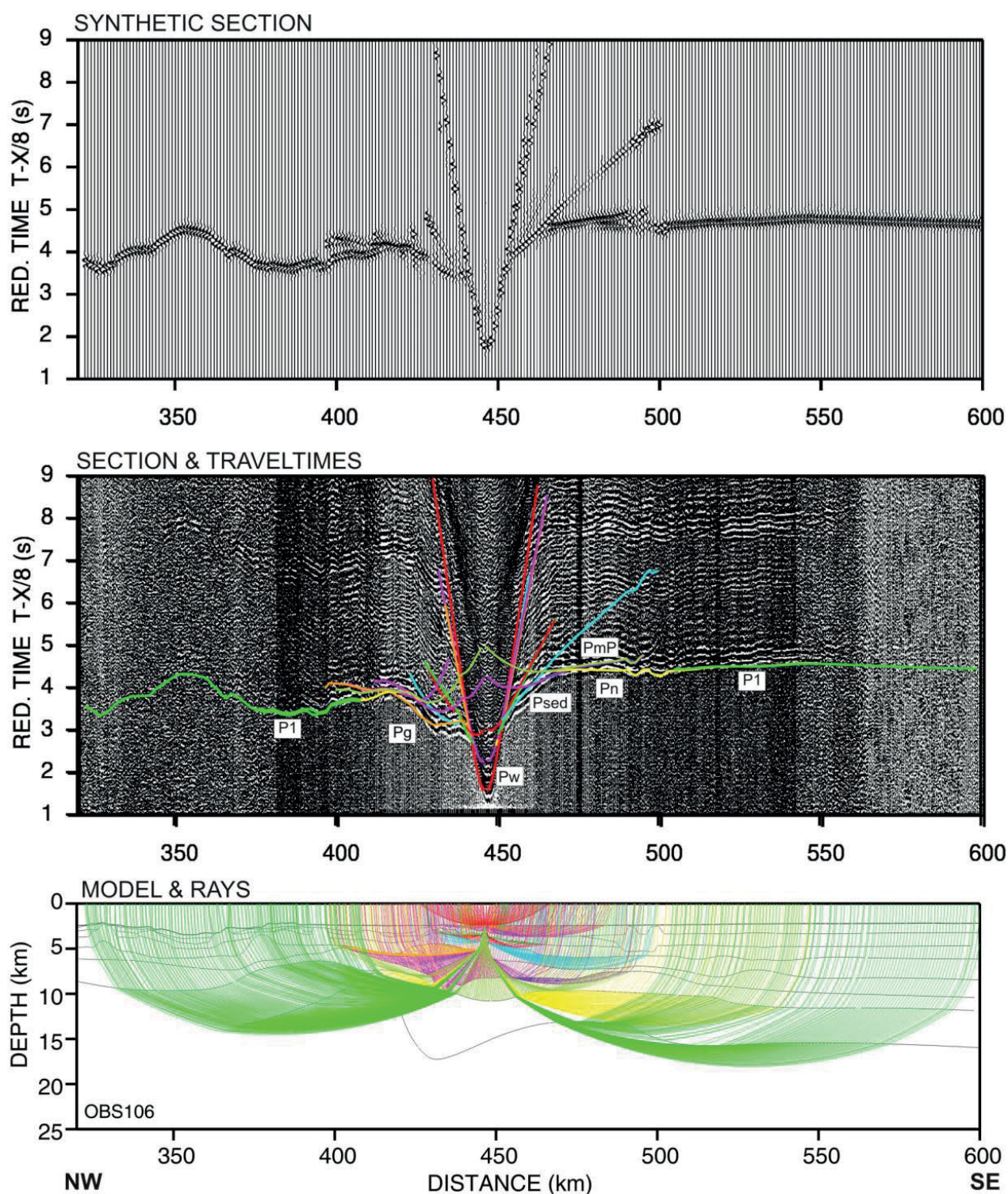


Fig. 7. Example of the 2-D seismic modelling along the KNIPSEIS profile for amplitude-normalized record section of OBS 106: model with rays (bottom), observed record sections (vertical-component) with calculated travel times (middle) and synthetic seismograms (top). PmP – Moho P-wave reflections. Other explanations as in Fig. 6.

4 km with P-wave velocities of 1.95, 2.90 to 3.85 km/s. The first sedimentary layer with the lowest velocity is *ca.* 1 km thick. In the Knipovich Ridge area, the crust is thinner, especially for the mid- and lower crust layers. The greatest uplift of the Moho boundary does not occur exactly beneath the Knipovich Ridge axis, but *ca.* 30 km to the SE, where

the thickness of the crust has been determined to be only 4 km. In the transition zone between the rift zone and the older oceanic crust, an increase in crustal thickness and an extension of the layer with a P-wave velocity of 6.7 km/s to a thickness of up to 5 km is determined. Almost along the entire profile, a layer with a P-wave velocity of *ca.* 7.1 km/s

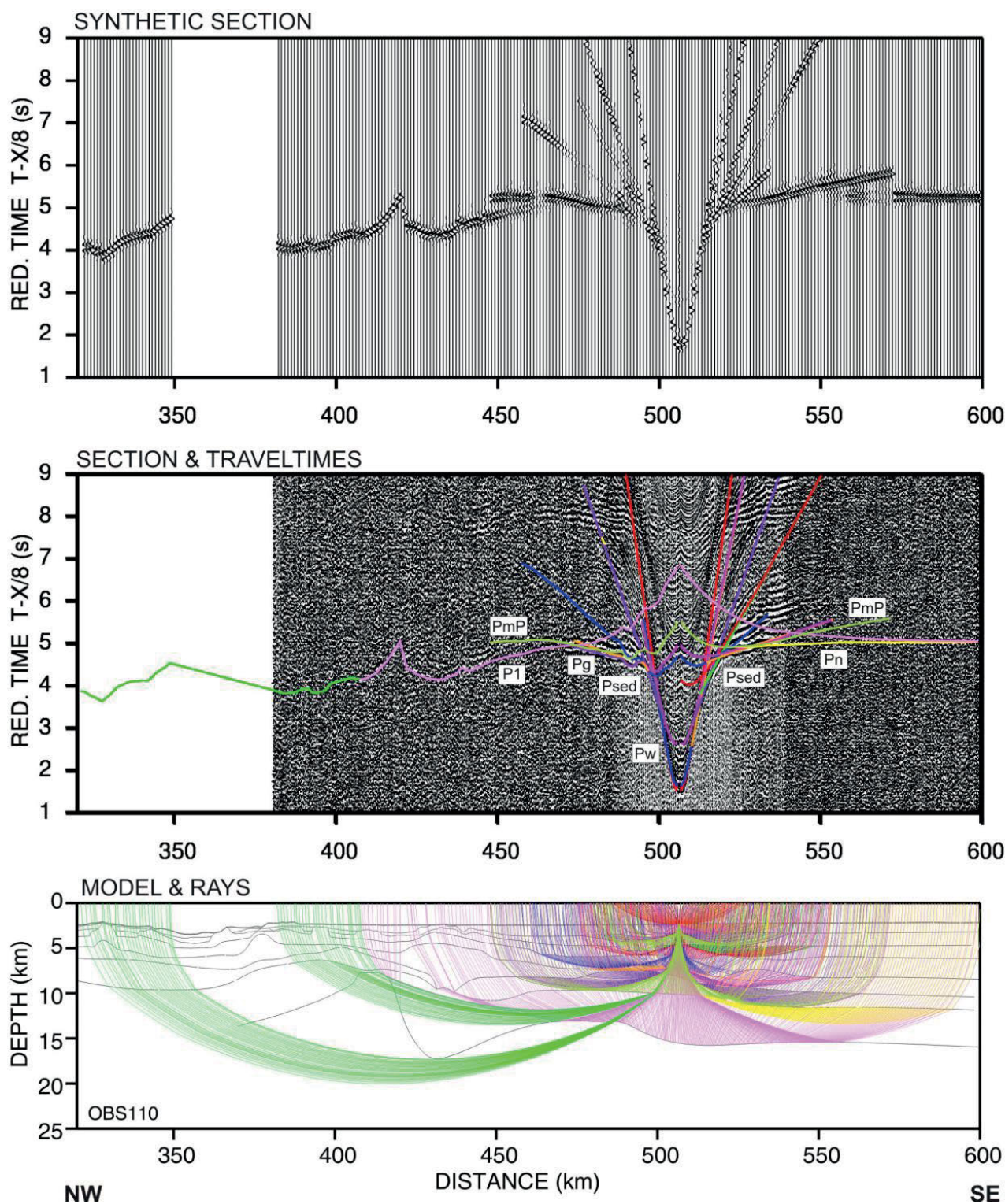


Fig. 8. Example of the 2-D seismic modelling along the KNIPSEIS profile for amplitude-normalized record section of OBS 110: model with rays (bottom), observed record sections (vertical-component) with calculated travel times (middle) and synthetic seismograms (top). Other explanations as in Fig. 6.

was found in the lower crust. P-wave velocities in the upper mantle were determined to be *ca.* 7.9 km/s in the Knipovich Ridge zone and 8.0 km/s beneath the oceanic crust at the SE part of the profile. The Moho depth varies from 6 km below OBS103 to 12 km at SE end of the profile. Its interface has

an undulating shape flattening at the SE end of the profile. In the upper mantle, the existence of a seismic boundary roughly replicating the shape of the Moho boundary was also additionally observed, with a P-wave velocity increased by 0.1 km/s. This boundary uplifts at the distance of 410 km

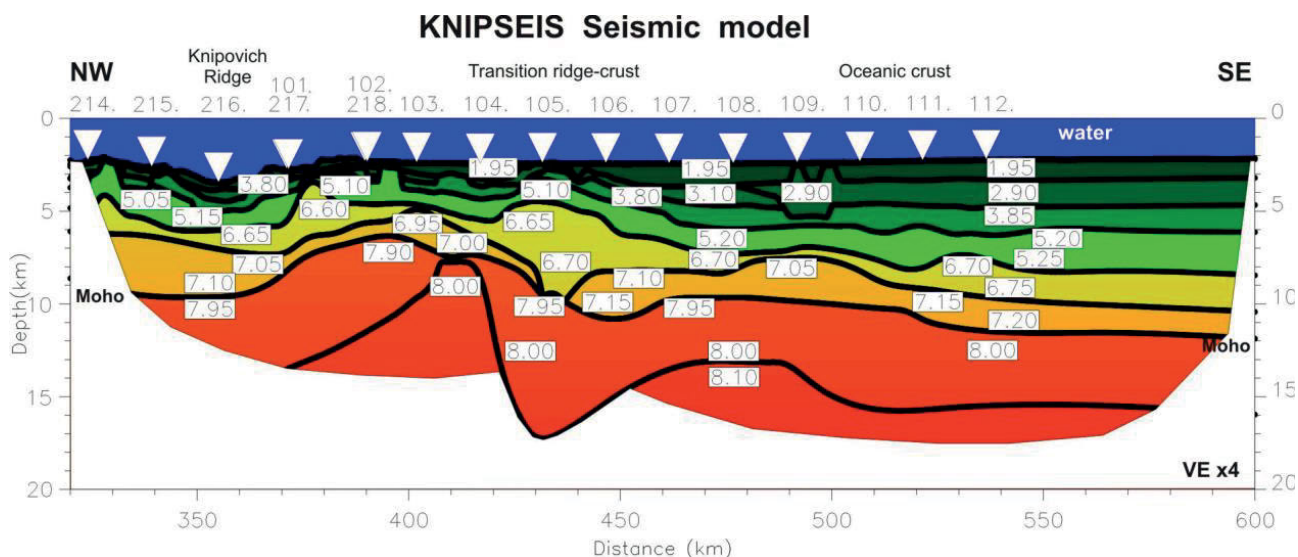


Fig. 9. Two-dimensional seismic P-wave velocity model along the KNIPSEIS profile developed by ray tracing technique. Vertical exaggeration 4:1. Triangles show location of OBSs with their numbers on top. Black lines represent seismic discontinuities (boundaries); colours represent the distribution of the P-wave velocity and numbers in the model are P-wave velocities in km/s.

almost reaching the Moho interface. There is determined several lower crustal boundaries shallowing together with Moho and the upper mantle interfaces at distances 460–510 km.

Discussion

We propose a conceptual subdivision of the profile into three main zones by correlating our results with modern models of oceanic crustal structure (Niu 2025, and references therein):

Zone A (> 7.90 km/s) – ultramafic upper mantle rocks, primarily peridotites. Mantle stratification in this zone is weakly expressed; however, we distinguish two sublayers characterized by relatively low internal velocity variation.

Zone B (7.20–5.05 km/s) – mafic oceanic crust. Within this zone, several sublayers can be identified based on distinct P-wave velocity contrasts, likely corresponding, from bottom to top, to gabbros, sheeted dike complexes, and basaltic pillow lavas. We interpret an interface with distinct increase in P-wave velocity to 7.9–8.0 km/s as the Moho discontinuity.

Zone C (1.95–3.85 km/s) – sediments.

It is important to note that the above subdivision is generalized and should be considered as a working model. In the transitional zone between the mantle and the oceanic crust, a number of geological processes affect the structure and physio-chemical properties of the rocks, influencing seismic wave propagation. These processes include mantle depletion due to the extraction of basaltic melt, potentially corresponding to the 7.95–8.00 km/s P-wave velocities on Fig. 9 (Zhang *et al.* 2022), and melt infiltration into mantle peridotites, possibly represented by the 7.05–7.20 km/s layer on Fig. 9 (Hidas *et al.* 2021). Additionally, in the context of ultraslow spreading ridges, deeply penetrating seawater can be heated by the cooling mantle, potentially

leading to localized or widespread serpentinization, further modifying the seismic properties of the lithosphere (Niu 2025).

The geometry of the analysed profile is variable. The structurally most complex part corresponds to the youngest section of the profile, located beneath the Knipovich Ridge and in its immediate vicinity (Dumais *et al.* 2021). The maximum mantle uplift along the profile does not occur directly beneath the ridge axis, but *ca.* 30 km to the SE, beneath OBS stations 102–103. The presence of amagmatic segments within ultraslow-spreading ridge systems has been documented in numerous studies, *e.g.*, Hellevang and Pedersen (2005) and Meier *et al.* (2022). Other authors have also highlighted that volcanism in such rift environments tends to occur over extended timescales and is not restricted to the axial zone alone (Stubseid *et al.* 2023).

Beneath OBS105, a significant thickening of the 6.60–6.70 km/s velocity layer is observed. This part of the profile may represent a relic magma chamber filled with gabbroic material. The chamber appears to be underlain by mantle material with slightly reduced seismic velocities (7.90–8.00 km/s), which reaches its greatest thickness directly beneath the interpreted chamber. These features support the interpretation that this section of the profile represents a phase of intense mafic magmatism, involving substantial melt transfer from the mantle into the crust and associated mantle depletion.

Further east of OBS106, the profile shows significantly reduced variability in the thicknesses of the defined seismic horizons. Nonetheless, some heterogeneity persists, suggesting that oscillatory magmatic activity may have also occurred during earlier stages of rift development. A gradual increase in the thickness of the uppermost oceanic sediment layer is observed toward the SE, a pattern consistent with enhanced terrigenous sediment input from the continental margin.

The crustal structure is roughly similar to other models located from the Knipovich Ridge region towards east (Czuba 2013). Hermann and Jokat (2013) presented the seismic model with similar upper crustal P-wave velocities but without the *ca.* 7 km/s layer. Also, the Moho depth determination is different, being shallower (6–8 km deep while in this study it is 6–12 km deep). The depth 6 km is similar and it is located on both sides of the ridge valley. Also, the mantle P-wave velocity is lower (7.5 vs. 7.9 km/s in this study). Comparing this study to the other models (Ljones *et al.* 2004; Czuba 2013), the Moho interface is at similar depth. The layer with P-wave velocity *ca.* 7 km/s does not exist only along several profiles located at the northern Knipovich Ridge. The mentioned profiles (Fig. 1) are located generally east of the Knipovich Ridge while the AWI-20090200 profile (Hermann and Jokat 2013) is located mainly west of the Knipovich Ridge and it could be the reason, connected with different behaviour of the crust towards Greenland.

Conclusions

The new wide-angle reflection and refraction seismic profile KNIPSEIS was realized in the North Atlantic at the ultra-slow oblique Knipovich Ridge toward SE. This paper presents the results of a deep seismic sounding experiment conducted along an *ca.* 300 km long transect between the Knipovich Ridge and the eastern margins of the North Atlantic abyssal plain. The P-wave velocity seismic crustal model was determined with an upper mantle boundary observed. The geometry of the interpreted seismic horizons along the profile, which records *ca.* 20 million years of seafloor spreading, exhibits significant variability, a characteristic feature of ultraslow rift systems. The observed variations in the thickness of individual horizons are likely related to variable intensities of magmatic processes, including the modification of the upper mantle through mechanisms such as mantle depletion or melt infiltration, occurring at various stages of rift evolution. Along the studied profile, the Moho discontinuity reaches its shallowest depth not directly beneath the Knipovich Ridge, but *ca.* 30 km to the SE. At this location, the crustal thickness is reduced to *ca.* 4 km only. The Moho interface determination is the basic result of this study. It is planned to join and remodel the profiles AWI-20090200 and KNIPSEIS to constitute a transect crossing the Knipovich Ridge to both directions towards Europe and Greenland.

Acknowledgements

We express our gratitude to Rolf Mjelde for his help in organizing the project as well as to Krzysztof Nejbert for valuable discussions. This work is supported by the National Science Centre, Poland according to the agreement UMO-2017/25/B/ST10/00488. The cruise was funded by University of Bergen. We thank the RV G. O Sars captain and the ship's crew. We thank the technician crew from the University of Bergen and the Institute of Geophysics PAS. The authors appreciate the valuable remarks of the reviewers.

References

- Canales L. 1984. Random noise reduction. *54th Annual International Meeting, SEG*. Expanded Abstracts: 525–527.
- Czuba W. 2013. Seismic View on the Svalbard Passive Continental Margin. *Acta Geophysica* 61: 1088–1100, doi: 10.2478/s11600-013-0126-0.
- Czuba W., Grad M. and Guterch A. 1999. Crustal structure of north-western Spitsbergen from DSS measurements. *Polish Polar Research* 20: 131–148.
- Czuba W., Grad M., Guterch A., Majdański M., Malinowski M., Mjelde R., Moskalik M., Środa P., Wilde-Piórko M. and Nishimura Y. 2008. Seismic crustal structure along the deep transect Horsted'05, Svalbard. *Polish Polar Research* 29: 279–290.
- Curewitz D., Okino K., Asada M., Baranov B., Gusev E. and Tamaki K. 2010. Structural analysis of fault populations along the oblique, ultra-slow spreading Knipovich Ridge, North Atlantic Ocean, 74°30'N–77°50'N. *Journal of Structural Geology* 32: 727–740, doi: 10.1016/j.jsg.2009.08.011.
- Červený V. and Pšenčík I. 1983. 2-D seismic ray tracing package SEIS83 (software package). Charles University, Prague.
- DeMets C., Gordon R.G., Argus D.F. and Stein S. 1990. Current plate motions. *Geophysical Journal International* 101: 425–478, doi: 10.1111/j.1365-246X.1990.tb06579.x.
- Dick H.J.B., Lin J. and Schouten H. 2003. An ultraslow-spreading class of ocean ridge. *Nature* 426: 405–412, doi: 10.1038/nature02128.
- Dumais M.-A., Gernigon L., Olesen O., Johansen S.E. and Brönnner M. 2021. New interpretation of the spreading evolution of the Knipovich Ridge derived from aeromagnetic data. *Geophysical Journal International* 224: 1422–1428, doi: 10.1093/gji/ggaa527.
- Gaina C., Jakobsson M., Straume E.O., Timmermans M.-L., Boggild K., Bünz S., Schlindwein V. and Døssing A. 2025. Arctic Ocean bathymetry and its connections to tectonics, oceanography and climate. *Nature Reviews Earth & Environment* 6: 211–227, doi: 10.1038/s43017-025-00647-0.
- Gernigon L., Franke D., Geoffroy L., Schiffer C., Foulger G.R. and Stoker M. 2020. Crustal fragmentation, magmatism, and the diachronous opening of the Norwegian-Greenland Sea. *Earth-Science Reviews* 206: 102939, doi: 10.1016/j.earscirev.2020.102939.
- Górszczyk A., Adamczyk A. and Malinowski M. 2014. Application of curvelet denoising to 2D and 3D seismic data—practical considerations. *Journal of Applied Geophysics* 105: 78–94, doi: 10.1016/j.jappgeo.2014.03.009.
- Grad M., Jensen S.L., Keller G.R., Guterch A., Thybo H., Janik T., Tiira T., Yliniemi J., Luosto U., Motuza G., Nasedkin V., Czuba W., Gaczyński E., Środa P., Miller K.C., Wilde-Piórko M., Komminaho K., Jacyna J. and Korabliova L. 2003. Crustal structure of the Trans-European suture zone region along POLONAISE'97 seismic profile P4. *Journal of Geophysical Research* 108, B11: 2541, doi: 10.1029/2003JB002426.
- Grad M., Guterch A., Keller G.R., Janik T., Hegedűs E., Vozár J., Ślaczka A., Tiira T. and Yliniemi J. 2006. Lithospheric structure beneath trans-Carpathian transect from Precambrian platform to Pannonian basin: CELEBRATION 2000 seismic profile CEL05. *Journal of Geophysical Research* 111: B03301, doi: 10.1029/2005JB003647.
- Grad M., Guterch A., Mazur Z., Keller G.R., Špičák A., Hrubcová P. and Geissler W.H. 2008. Lithospheric structure of the Bohemian Massif and adjacent Variscan belt in central Europe based on profile S01 from the SUDETES 2003 experi-

- ment. *Journal of Geophysical Research* 113: B10304, doi: 10.1029/2007JB005497.
- Grevemeyer I., Ranero C.R. and Ivandic M. 2018. Structure of oceanic crust and serpentinisation at subduction trenches. *Geosphere* 14: 1–23, doi: 10.1130/GES01537.1.
- Hellevang B. and Pedersen R.B. 2005. Magmatic segmentation of the northern Knipovich Ridge: Evidence for high-pressure fractionation at an ultraslow spreading ridge. *Geochemistry, Geophysics, Geosystems* 6: Q09007, doi: 10.1029/2004GC000898.
- Hermann T. and Jokat W. 2013. Crustal structures of the Boreas Basin and the Knipovich Ridge, North Atlantic. *Geophysical Journal International* 193: 1399–1414, doi: 10.1093/gji/ggt048.
- Hidas K., Borghini G., Tommasi A., Zanetti A. and Rampone E. 2021. Interplay between melt infiltration and deformation in the deep lithospheric mantle (External Liguride ophiolite, North Italy). *Lithos* 380–381: 105855, doi: 10.1016/j.lithos.2020.105855.
- Jakobsson M., Cherkis N.Z., Woodward J., Macnab R. and Coakley B. 2000. New grid of Arctic bathymetry aids scientists and mapmakers. *EOS Transactions, AGU* 81: 89, 93, 96.
- Janik T., Yliniemi J., Grad M., Thybo H., Tiira T. and POLONAISE P2 Working Group 2002. Crustal structure across the TESZ along POLONAISE '97 seismic profile P2 in NW Poland. *Tectonophysics* 360: 129–152, doi: 10.1016/S0040-1951(02)00353-0.
- Jokat W. and Schmidt-Aursch M. 2007. Geophysical characteristics of the ultraslow spreading Gakkel Ridge, Arctic Ocean. *Geophysical Journal International* 168: 983–998, doi: 10.1111/j.1365-246X.2006.03278.x.
- Kandilarov A., Landa H., Mjelde R., Pedersen R., Okino K. and Murai Y. 2010. Crustal structure of the ultra-slow spreading Knipovich Ridge, North Atlantic, along a presumed ridge segment center. *Marine Geophysical Researches* 31: 173–195, doi: 10.1007/s11001-010-9095-8.
- Komminaho K. 1997. Software manual for programs MODEL and XRAYS—a graphical interface for SEIS83 program package. University of Oulu, Department of Geophysics, Report 20: 1–31.
- Krysiński L., Grad M., Mjelde R., Czuba W. and Guterch A. 2013. Seismic and density structure of the lithosphere–asthenosphere system along transect Knipovich Ridge–Spitsbergen–Barents Sea – geological and petrophysical implications. *Polish Polar Research* 34: 111–138, doi: 10.2478/popore-2013-0011.
- Ljones F., Kuwano A., Mjelde R., Breivik A., Shimamura H., Murai Y. and Nishimura Y. 2004. Crustal transect from the North Atlantic Knipovich Ridge to the Svalbard Margin west of Hornsund, *Tectonophysics* 378: 17–41, doi: 10.1016/j.tecto.2003.10.003.
- Meier M., Schlindwein V. and Schmid F. 2022. Magmatic activity and dynamics of melt supply of volcanic centers of ultraslow spreading ridges: Hints from local earthquake tomography at the Knipovich Ridge. *Geochemistry, Geophysics, Geosystems* 23: e2021GC010210, doi: 10.1029/2021GC010210.
- Mjelde R., Breivik A.J., Elstad H., Ryseth A.E., Skilbrei J.R., Opsal R.R., Shimamura H., Murai Y. and Nishimura Y. 2002. Geological development of the Sørvestsnaget Basin, SW Barents Sea, from ocean bottom seismic, surface seismic and potential field data. *Norwegian Journal of Geology* 82: 183–202.
- Niu Y. 2025. Shallow origin of continental mantle materials beneath slow-spreading ocean ridges. *Science Bulletin (Beijing)* 70: 1533–1537, doi: 10.1016/j.scib.2025.01.028.
- Peacock K.L. and Treitel S. 1969. Predictive deconvolution: theory and practice, *Geophysics* 34, 155–169, doi: 10.1190/1.1440003.
- Ritzmann O., Jokat W., Mjelde R. and Shimamura H. 2002. Crustal structure between the Knipovich Ridge and the Van Mijenfjorden (Svalbard). *Marine Geophysical Researches* 23: 379–401, doi: 10.1023/B:MARI.0000018168.89762.a4.
- Stubseid H. H., Bjerga A., Haflidason H., Pedersen L.E.R. and Pedersen R.B. 2023. Volcanic evolution of an ultraslow-spreading ridge. *Nature Communications* 14: 4134, doi: 10.1038/s41467-023-39925-0.
- Środa P., Czuba W., Grad M., Guterch A., Tokarski A.K., Janik T., Rauch M., Keller G.R., Hegedűs E., Vozár J. and CEL-EBRATION 2000 Working Group. 2006. Crustal and upper mantle structure of the Western Carpathians from CELEBRATION 2000 profiles CEL01 and CEL04: seismic models and geological implications. *Geophysical Journal International* 167: 737–760, doi: 10.1016/j.jog.2010.12.002.
- Talwani M. and Eldholm O. 1977. The evolution of the Norwegian-Greenland Sea: recent results and outstanding problems. *Geological Society of America Bulletin* 88: 969–999, doi: 10.1130/0016-7606(1977)88<969:EOTNS>2.0.CO;2.
- Trojanowski J., Górszczyk A. and Eisner L. 2016. A multichannel convolution filter for correlated noise: Microseismic data application. *SEG Technical Program*. Expanded Abstracts: 2637–2641.
- Van Avendonk H.J.A., Davis J.K., Harding J.L. and Lawver L.A. 2017. Decrease in oceanic crustal thickness since the breakup of Pangaea. *Nature Geoscience* 10: 58–61. doi: 10.1038/ngeo2849.
- Wessel P. and Smith W.H.F. 1998. New, improved version of the Generic Mapping Tools released. *EOS, Transactions American Geophysical Union* 79: 579, doi: 10.1029/98EO00426.
- Wessel P., Smith W.H.F., Scharroo R., Luis J. and Wobbe F. 2013. Generic Mapping Tools: Improved Version Released. *EOS, Transactions American Geophysical Union* 94: 409–410, doi: 10.1002/2013EO450001.
- White R.S., Minshull T.A., Bickle M. and Robinson C.J. 2001. Melt Generation at Very Slow-Spreading Oceanic Ridges: Constraints from Geochemical and Geophysical Data. *Journal of Petrology* 42: 1171–1196, doi: 10.1093/petrology/42.6.1171.
- Zelt C.A. 1994. Software package ZPLOT. Bullard Laboratories, University of Cambridge, Cambridge.
- Zhang W.-Q., Liu C.-Z., Mitchell R.N., Liu T., Zhang C. and Zhang Z.-Y. 2022. Extensive melting of ancient depleted oceanic mantle evidenced by decoupled Hf–Nd isotopes in the lowermost oceanic crust. *Lithos* 418–419: 106684, doi: 10.1016/j.lithos.2022.106684.